ISIJ International, Vol. 58 (2018), No. 4, pp. 686–695

# A Reaction between High Mn–High Al Steel and CaO–$SiO_2$-Type Molten Mold Flux: Reaction Mechanism Change by High Al Content ($[pct\ Al]_0 = 5.2$) in the Steel and Accumulation of Reaction Product at the Reaction Interface

Min-Su KIM,[1,2] Min-Seok PARK,[3] Shin-Eon KANG,[3] Joong-Kil PARK[3] and Youn-Bae KANG[1]*

1) Graduate Institute of Ferrous Technology, Pohang University of Science and Technology, Pohang, Kyungbuk, 37673 Rep. of Korea. 2) Jeonbuk Regional Division, Korean Institute of Industrial Technology, Kimje, Jeonbuk, 54325 Rep. of Korea. 3) Kwangyang Process Research Group, Technical Research Laboratories, POSCO, Kwangyang, Jeonnam, 57807 Rep. of Korea.

(*Received on October 24, 2017; accepted on December 5, 2017*)

A series of laboratory-scale experiments were carried out in order to elucidate the reaction mechanism between high Mn-high Al steel and CaO–$SiO_2$-type molten mold flux at 1 450°C, which represents the reaction taking place during continuous casting of the steel. Compared to the previous study [Kim *et al.*, Metall. Mater. Trans. 44B (2013) 299–308], high Al content in the liquid steel ($[pct\ Al]_0 = 5.2$) and high MgO content in the liquid flux ($(pct\ MgO)_0 = 5$ to 15) were employed, in order to confirm change of rate-controlling step from mass transport of Al in liquid steel to more complicated steps including mass transport in liquid flux. It was found that $Al_2O_3$ was rapidly accumulated near the interface of the flux, and $SiO_2$ and $Na_2O$ were reduced simultaneously, regardless of $(pct\ MgO)_0$. At the early stage of the reaction (1 min), $MgAl_2O_4$ particles were observed in the flux near the interface, then the particles were spreading out into the bulk flux as the reaction time passed. Other solid phases ($CaAl_4O_7$, $Al_2O_3$) were also observed due to local depletion of MgO in the flux. The $MgAl_2O_4$ formation mechanism and its effect on mass transfer in the molten flux were discussed. A series of simple kinetic analyses showed that the mass transport of Al in liquid steel is no more controlling the reaction rate. It was concluded that there were possibilities of mass transport in the flux phase contributing reaction rate controlling step.

KEY WORDS: flux-steel reaction; reaction mechanism; $Al_2O_3$ accumulation; high Mn-high Al steel; CaO–$SiO_2$-type mold flux.

## 1. Introduction

High performance light weight steel has been developed, which consists of high Mn and high Al contents. Continuous casting of this steel grade inevitably involves reaction between the high Mn-high Al steel and CaO–$SiO_2$ type molten mold flux in the casting mold. The present authors investigated a reaction mechanism between the high Mn-high Al steel and the CaO–$SiO_2$ type molten mold flux, and it was shown that the following reaction was mostly taking place:[1,2]

$$4\underline{Al} + 3(SiO_2) = 3\underline{Si} + 2(Al_2O_3) \quad \ldots\ldots\ldots\ldots\ldots (1)$$

Additional oxidation and reduction of $Fe_tO$ and MnO were observed.[1] Employed flux was composed of CaO–$SiO_2$–$Al_2O_3$–MgO–$Na_2O$–F of various (pct CaO)/(pct $SiO_2$) ratios, (pct $Al_2O_3$).[1] Reaction rate between the steel and the flux was limited by mass transport of Al in the liquid steel, when the initial content of Al, $[pct\ Al]_0$, was not higher than 1.8, in the temperature range of 1 440°C to 1 550°C. It was found that the rate controlling step was no more valid when $[pct\ Al]_0$ was 4.8. Moreover, the flux after the reaction was no more homogeneous, but $MgAl_2O_4$ solid phases were observed near interface between the steel and the flux. This observation was also reported by Kim and Park for reaction between Fe–Mn–Al alloy and CaO–MgO–$SiO_2$–$Al_2O_3$ slag at 1 600°C.[3] The reaction product ($MgAl_2O_4$) accumulated at the interface, and it was thought that it may retard the reaction between the steel and the flux. In the previous research, only experimental data of low Al content was utilized in the development of rate equation in order to predict composition evolution in the mold flux during the continuous casting.[2]

Accumulation of the reaction product $MgAl_2O_4$ is due to the high Al content in the steel and the MgO in the flux. As new grade of lightweight steel requires high Al content as high as ~10 mass pct.,[4] and MgO is generally introduced as impurities from raw materials, it is likely that rapid reaction between Al in liquid steel and $SiO_2$ in the flux takes place, followed by formation of $MgAl_2O_4$ or other solid phases.

* Corresponding author: E-mail: ybkang@postech.ac.kr
DOI: http://dx.doi.org/10.2355/isijinternational.ISIJINT-2017-603

This influences composition of remained mold flux, and may change transport property of the liquid flux by changing viscosity. Then it results in shifting rate controlling step from mass transport in liquid steel to mass transport in liquid flux. Previous investigations on $SiO_2$ reduction by Al in liquid Fe are summarized in **Table 1**.[1–3,5–8] Some including the present authors reported that mass transport of Al in liquid steel was rate controlling step,[2,5,6] while others reported chemical reaction[7] or mixed control (mass transport in both phases).[8] It is thought that the rate controlling step during the reaction may not be permanent during the reaction. Depending on the flux chemistry and the reaction product, the rate controlling step would shift to mass transport in the liquid flux.

Since reduction of $SiO_2$ and accumulation of $Al_2O_3$ in the flux during continuous casting deteriorate cast product quality and process efficiency, prevention of the reaction is required.[9,10] Understanding reaction mechanism between the high Mn-high Al steel and $CaO–SiO_2$ type mold flux is therefore important, and prediction of the evolution of flux composition would be useful, which may further be utilized to assess functions of the mold flux (crystallization, fluidity, heat transfer, lubrication, *etc.*). The present article is one of continuing contributions of the present authors in order to understand reactions between the high Mn-high Al steel and $CaO–SiO_2$ type molten mold flux. Experimental set up and general reaction phenomena for relatively lower $[pct\ Al]_0$ (less than 1.8) was presented in Reference 1). Elucidation of reaction mechanism, interfacial morphology, and a simply kinetic model was discussed in Reference 2). The kinetic model was developed in the regime of liquid steel mass transport control due to the relatively lower $[pct\ Al]_0$. In the present article, it is shown how the rate controlling step is changed by accumulation of reaction product at the interface. This is induced by higher $[pct\ Al]_0$ in the steel and higher $(pct\ MgO)_0$ in the flux. All these results can be utilized in order to develop a general reaction model which takes into account reaction kinetics controlled by mass transport in both phases (liquid steel and molten mold flux) and effect of changing the flux composition on mass transfer coefficient.

## 2. Experimental

### 2.1. Sample Preparation

Steel sample was prepared by weighing desired amounts of electrolytic iron (99.99 pct, Toho Zinc Co. Ltd., Tokyo, Japan), manganese chip (99.99 pct, LTS Chemical Inc., Orangeburg, NY, USA), aluminum granule (99.99 pct, Kojundo Chemical Co., Saitama, Japan). Fe–C alloy ([pct C] = 5) was prepared separately by melting the electrolytic iron and C powder in a graphite crucible in an induction melting furnace. Pre-fused fluxes with three different $(pct\ MgO)_0$ (= 5, 10, 15) were prepared by weighing $CaCO_3$ (98.0 pct, Kanto chemicals, Tokyo, Japan), $SiO_2$ (extra pure, Kanto chemicals, Tokyo, Japan), $Al_2O_3$ (99.0 pct, Kanto chemicals, Tokyo, Japan), and MgO (98.0 pct, Kanto chemicals, Tokyo, Japan) in desired proportions, melting in a graphite crucible in an induction furnace. The liquid flux was then quenched on a stainless steel plate cooled by water, and it was ground into powder. $CaF_2$ (98.0 pct, Kanto chemicals, Tokyo, Japan) and $Na_2CO_3$ (99.5 pct, Kanto chemicals, Tokyo, Japan) were then mixed with the pre-fused flux powder. Initial compositions of the steel and the flux samples were given in **Table 2**.

### 2.2. Sampling Experiment

In order to measure composition change during reaction between molten steel and molten flux, a series of sampling experiment were carried out. Schematic diagram for sampling experiments is shown in **Fig. 1**(a). 400 g of the prepared steel sample was charged in an $Al_2O_3$ crucible (OD 60 mm × ID 52 mm × H 100 mm) and melted in an induction furnace equipped with a quartz reaction tube and

**Table 1.** Summary of kinetic studies on $SiO_2$ reduction in molten slags/fluxes by Al in liquid Fe.

| Author | Ooi *et al.*[7] | Sun and Mori[5] | Rhamdhani *et al.*[6] | Kim and Park[3] | Park *et al.*[8] | Kim *et al.*[1,2] |
|---|---|---|---|---|---|---|
| Steel comp. (mass pct) | Fe-4Al | Fe-(0.25-0.4)Al | Fe-(3.5-5)Al | Fe-(1,3,6)Al-(10-20)Mn | Fe-(0.057-0.45)Al | Fe-13Mn-(0.4-4.8) Al-(0.4-1.7)Si-0.65C |
| Slag comp. (mass pct.) | 40CaO-40$SiO_2$-20$Al_2O_3$ | CaO-$Al_2O_3$-(5,10) $SiO_2$-FeO-MnO (C/A = 1) | 40CaO-40$SiO_2$-20$Al_2O_3$ | 30CaO-60$SiO_2$-5$Al_2O_3$-5MgO | 34CaO-5$SiO_2$-47$Al_2O_3$-14MgO | (17-37)CaO-(31-53) $SiO_2$-(0-12)$Al_2O_3$-2.5MgO-14$Na_2O$-7.7F |
| Temperature (°C) | 1 570 | 1 600 | 1 550–1 650 | 1 600 | 1 600 | 1 440–1 550 |
| Experimental method | Steel droplet in liquid slag pool | Slag injection on liquid steel pool | Steel droplet in liquid slag pool | Slag injection on liquid steel pool | Slag injection on liquid steel pool | Slag injection on liquid steel pool |
| Rate controlling step | $SiO_2$ reduction at steel-slag interface | Mass transfer of Al in liquid steel | Mass transfer of Al in liquid steel | – | Mixed transport control | Mass transfer of Al in molten steel ($[pct\ Al]_0 \leq 1.8$) |
| Mass transfer coefficient of Al (m $sec^{-1}$) | – | $2.2–8.1 \times 10^{-4,*}$ | $1.3–1.9 \times 10^{-6}$ | $3.6 \times 10^{-4}–1.5 \times 10^{-2}$ | $6 \times 10^{-5}$ | $\exp\left(-\frac{14\,200}{T}-1.1107\right)$ |
| Activation energy (kJ $mol^{-1}$) | – | – | 127 | – | – | 119 |
| Steel & slag comp. range | High Al High $SiO_2$ | Low Al Low $SiO_2$ | High Al High $SiO_2$ | Low-high Al High $SiO_2$ | Low Al Low $SiO_2$ | Low-high Al High $SiO_2$ |

*Calculated by the present authors from $k_{Al}^{m}\rho_{steel}$ with assumption ($\rho_{steel}$ = 6 800 kg $m^{-3}$).

**Table 2.** Initial compositions of steel and flux samples used in the present study (mass pct).

| Fe | C | Al | Si | Mn |
|---|---|---|---|---|
| Bal. | 1.00 | 5.17 | 0.024 | 20.76 |

| Sample | CaO | $SiO_2$ | $Al_2O_3$ | MgO | $Na_2O$ | F |
|---|---|---|---|---|---|---|
| F-5M | 32.48 | 34.51 | 5.97 | 5.00 | 14.17 | 7.86 |
| F-10M | 27.48 | 34.51 | 5.97 | 10.00 | 14.17 | 7.86 |
| F-15M | 22.48 | 34.51 | 5.97 | 15.00 | 14.17 | 7.86 |

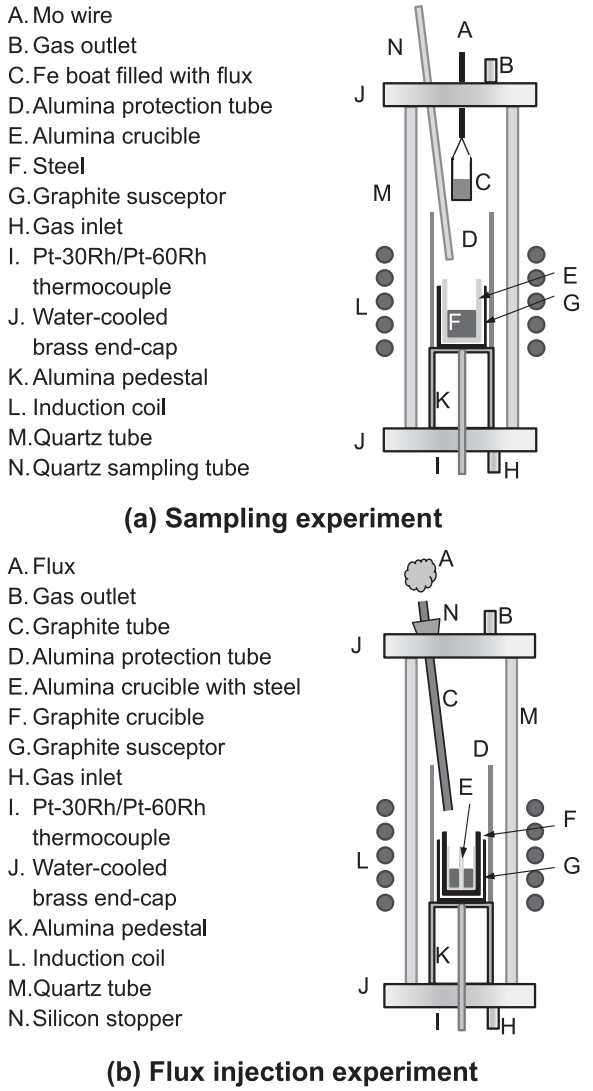


**Fig. 1.** Schematic diagrams of experimental apparatus for (a) the sampling experiments and (b) the flux injection experiment.

water-cooled brass end caps. When the steel sample was fully melted, the melt temperature was adjusted to 1 450°C by using a B-type thermocouple inserted in the melt. After 30 minutes for homogenization, small amount of steel melt was sampled by using a quartz tube (OD 6 mm × ID 4 mm × H 60 mm) and rapidly quenched into cold water in order to check initial composition of steel. 40 g of flux carried in a boat made from an iron foil was then dropped onto the molten steel in order to initiate the steel/flux reaction. It took about 1 minute for the flux assembly to fully melt. Reaction time was set to zero at this moment. Small amount of steel and flux were taken out periodically up to 20 minutes by using different quartz tubes (OD 6 mm × ID 4 mm × H 60 mm for steel, and OD 10 mm × ID 8 mm × H 60 mm for flux). Those were quenched into cold water. During the experiments, the atmosphere inside the furnace was controlled by supplying Ar gas (99.999 pct purity, further purified by passing through $CaSO_4$ and Mg chips at 500°C) in order to remove moisture and oxygen in the gas, respectively.

The steel samples were ground, cut, and analyzed by Inductively Coupled Plasma-Atomic Emission Spectroscopy (ICP-AES) in order to obtain Mn, Si, and Al concentrations in the steel. The flux samples were ground and subjected to X-Ray Flourescence (XRF) spectroscopy in order to obtain CaO, $SiO_2$, $Al_2O_3$, MgO, $Na_2O$, F, MnO, and FeO contents in the flux.

### 2.3. Flux Injection Experiment

Due to rapid $Al_2O_3$ accumulation in a CaO–$SiO_2$-type flux during the reaction, some aluminate could be formed near the steel/flux interface.[2] This changes concentration of remained molten flux, then may affect mass transport in the flux phase. Therefore examination of well-preserved steel/flux interface is essential in order to understand the reaction mechanism. Schematic diagram for flux injection experiments is shown in Fig. 1(b). Three $Al_2O_3$ crucibles (OD 18 mm × ID 15 mm × H 50 mm) containing 16.6 g of steel sample were located in a graphite holder, and put into the induction furnace. After the molten steel was homogenized at 1 450°C, the fluxes were dropped onto each molten steel through a carbon tube. After the desired reaction time (1, 2, and 4 minutes), the whole sample assembly was taken out of the furnace and quenched into the water. During water quenching, the steel/flux interface was carefully protected by covering the open ends of the $Al_2O_3$ crucibles with ceramic caps in order to prevent the sample from damaging by the quenching water.

After the samples were completely dried, those were cold-mounted, cut, and polished in order to examine vertical-sectional area of steel/flux interface. Mircrostructure observation was performed by Scanning Electron Microscope (SEM, JSM-5900, JEOL, Japan). Line scan analysis based on Wavelength-Dispersive Spectroscopy (WDS) was also conducted by using Electron Probe MicroAnalysis (EPMA, JXA-8100, JEOL, Japan).

In both experiments (Sec. 2.2 and Sec. 2.3), the use of $Al_2O_3$ crucible could result in additional accumulation of $Al_2O_3$ in the flux by corrosion of the crucible. In a series of preliminary test using different crucibles (MgO and $Al_2O_3$), it was found that the additional accumulation of $Al_2O_3$ in the flux was not significant to that caused by the chemical reaction between steel and flux. Therefore, the additional accumulation of $Al_2O_3$ caused by the use of $Al_2O_3$ crucible was ignored in the present study.

## 3. Results

### 3.1. Composition Evolution in the Steel-flux System

Typical composition evolutions in the molten steel and the flux ($(pctMgO)_0$ = 5) are shown in **Fig. 2**. Concentrations of Al in the steel and $SiO_2$ in the flux decreased, while

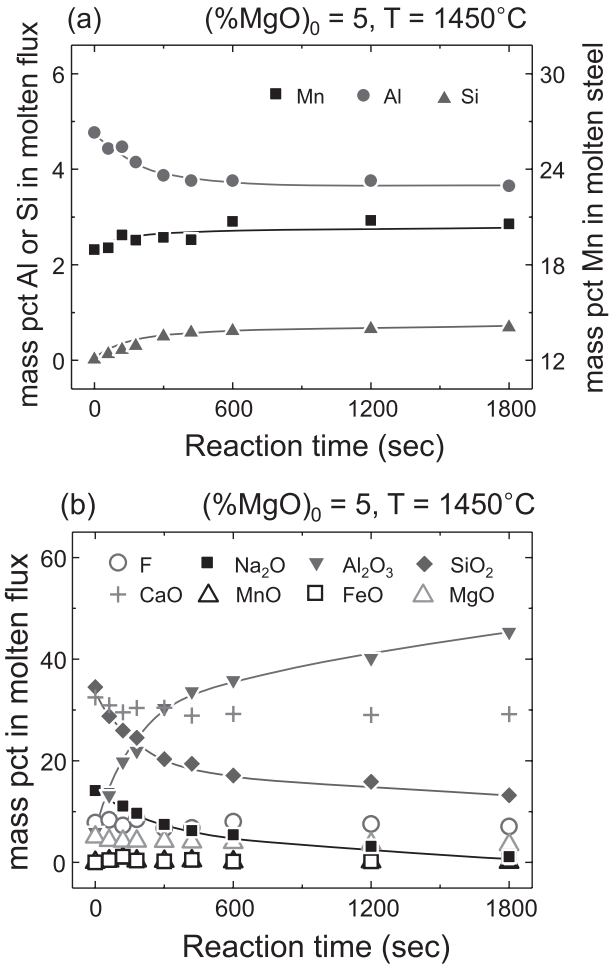


**Fig. 2.** Composition evolution in (a) molten steel and (b) molten flux at 1 450°C when (pct $MgO)_0$ was 5. Solid lines are to guide the eye.

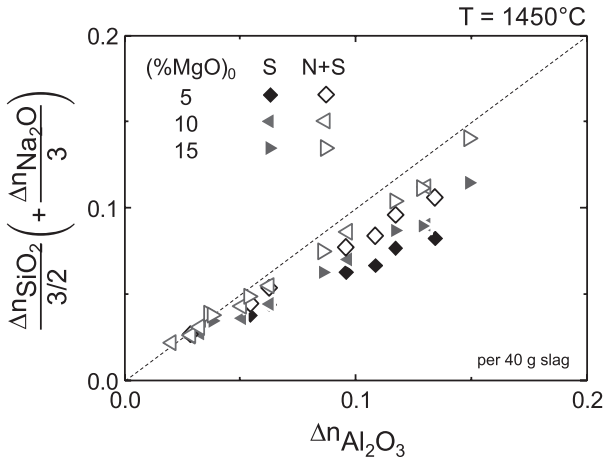


**Fig. 3.** Mass balance between $Al_2O_3$ and weak oxides ($SiO_2$ and $Na_2O$) reduced by Al at 1 450°C under various (pct $MgO)_0$ conditions. S: $Al_2O_3$ formation by reduction of $SiO_2$ only. N+S: $Al_2O_3$ formation by reduction of both $SiO_2$ and $Na_2O$.

Si in the steel and $Al_2O_3$ in the flux increased. This is consistent with the previous investigation,[1] and the Reaction (1) took place. In addition to this reaction, considerable amount of $Na_2O$ was also reduced: it was thought to be reduced mostly by Al. A similar result was observed at 1 500°C.[1] It was suggested the following reaction might occur:

$$2\underline{Al} + 3(Na_2O) = 6Na + (Al_2O_3) \quad \ldots\ldots\ldots\ldots\ldots (2)$$

where the reduced Na may be evaporated into gas phase.[1] In the present study, fume was observed in the reaction chamber (quartz tube) during the experiment. Deposits were found on inner surface of the reaction chamber. It was analyzed by EDS and was confirmed to contain Na. Since solubility of Na in liquid Fe is not accurately known but is thought to be very low due to high vapor pressure of Na, it can be concluded that Na in the above reaction was evaporated.

After 30 minutes of the reaction, $Al_2O_3$ concentration increased over 40 pct, while most of $Na_2O$ was reduced. Except for $Al_2O_3$, $SiO_2$, and $Na_2O$, other components in the flux were relatively stable. Similar evolution was observed when $(pctMgO)_0$ was 10 and 15, respectively. Therefore, it could be concluded that the dominant reactions between high Mn-high Al steel and CaO–$SiO_2$-type molten mold flux at high Al concentration (5.2 mass pct) and high MgO concentration (5–15 mass pct) are $Al_2O_3$ accumulation reaction coupled with $SiO_2$ and $Na_2O$ reduction (Reactions (1) and (2)).

This conclusion is also verified by mass balance between produced $Al_2O_3$ and reduced $SiO_2$ and $Na_2O$. **Figure 3** shows relationship between number of moles of produced $Al_2O_3$ ($\Delta n_{Al_2O_3}$), that of reduced $SiO_2$ ($\Delta n_{SiO_2}$), and that of reduced $Na_2O$ ($\Delta n_{Na_2O}$). Produced amount of $Al_2O_3$ could not be solely accounted for by reduced amount of $SiO_2$ as shown by closed symbols. Taking into account the reduction of $Na_2O$ (Reaction (2)) improved the mass balance calculation as shown by open symbols. Therefore, the validity of the Reaction (2) was verified. This is practically important result that decrease of $Na_2O$ content in mold flux increases viscosity of the flux and increases melting temperature of the flux. Therefore, gradual decrease of the $Na_2O$ content in mold flux during continuous casting of high Mn-high Al steel is expected to cause serious difficulties in practical operation. This is an additional source of trouble for continuous casting of high Mn-high Al steel, apart from the Reaction (1).

In order to investigate the effect of MgO on $Al_2O_3$ accumulation rate, composition evolutions of the reactant and the product of the reaction under different (pct $MgO)_0$ are compared in **Fig. 4**. It is expected that more (pct $MgO)_0$ in the mold flux would result in more $MgAl_2O_4$ to form. Composition evolutions in the molten steel and the flux did not show clear trend. Increasing (pct $MgO)_0$ from 5 to 10 decreased the reaction rate by examining composition evolution Al, Si, $Al_2O_3$, and $SiO_2$. However, further increasing (pct $MgO)_0$ to 15 increased the reaction rate. It is not clear at the present stage why the effect of MgO on the rate was not simple. Formation of $MgAl_2O_4$ in the flux, which will be shown in next section, might have played as resistance of mass transport in the flux, or as sink of $Al_2O_3$ accumulated in the flux.

Composition evolutions of other weak oxides such as $Na_2O$, MnO, and FeO are also shown in **Fig. 5**. Similar to the previous experimental results,[1] concentrations of MnO and FeO showed sharp increase at the beginning of the reaction, followed by rapid decrease, except for (% FeO) change when $(\%MgO)_0$ = 15, which looks certainly in error. From the high Mn in the molten steel and high $SiO_2$ in the flux, it could be expected that Mn was oxidized, coupled with

$SiO_2$ reduction:

$$2\underline{Mn} + (SiO_2) = \underline{Si} + 2(MnO) \quad \text{..... (3)}$$

Then, consequent reduction of MnO was followed due to high Al concentration in the molten steel:

$$2\underline{Al} + 3(MnO) = 3\underline{Mn} + (Al_2O_3) \quad \text{..... (4)}$$

At the initial stage of the steel-flux reaction, oxidation of Fe also took place and reduced back in 10 minutes of the reaction time. These observations are similar to what was observed in the previous study for low Al containing steel.[1)]

### 3.2. Interfacial Morphology of the Steel-flux Systems at Different (pct $MgO)_0$

**Figure 6** shows SEM images of mold flux near the steel-flux interface at each reaction time up to 4 minutes. Fluxes of different (pct $MgO)_0$ are shown. It is seen that smaller particles were found in the flux, and it was revealed to be $MgAl_2O_4$ by WDS analysis. At a given reaction time, number of the $MgAl_2O_4$ particles was more in the flux of higher (pct $MgO)_0$. For a given (pct $MgO)_0$, number of the $MgAl_2O_4$ particles increased as reaction time passed. And location of $MgAl_2O_4$ found gradually expanded away from the interface. The formation behavior of $MgAl_2O_4$ in the fluxes suggests that mass transport of $Al_2O_3$ from the interface to the bulk flux had occurred, but not as fast as to neglect resistance for the mass transport in the flux. Gradual change of $MgAl_2O_4$ forming location implies that there were non-ignorable concentration gradient. Development of the concentration gradient will be discussed in Sec. 4.1.

In addition to the $MgAl_2O_4$ particles, $CaAl_4O_7$, $Al_2O_3$, and $CaF_2$ phases were also observed near the interface as shown in **Fig. 7**. $MgAl_2O_4$ formation caused local depletion

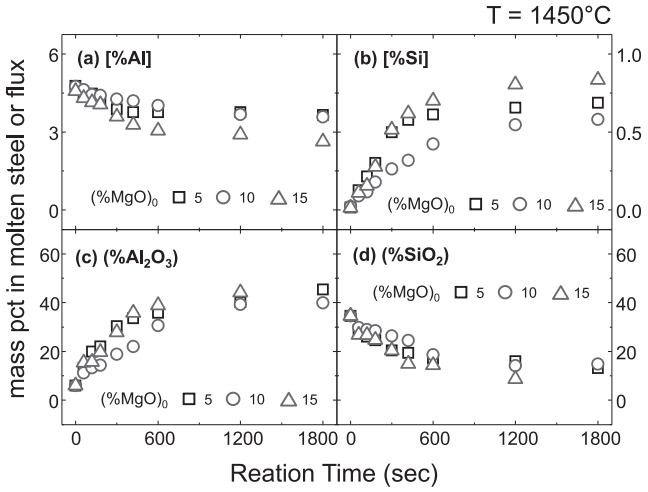


**Fig. 4.** Effect of (pct $MgO)_0$ on the composition evolution in the molten flux reacted with the molten steel at 1 450°C: (a) [pct Al] in molten steel, (b) [pct Si] in molten steel, (c) (pct $Al_2O_3$) in molten flux, and (d) (pct $SiO_2$) in molten flux.

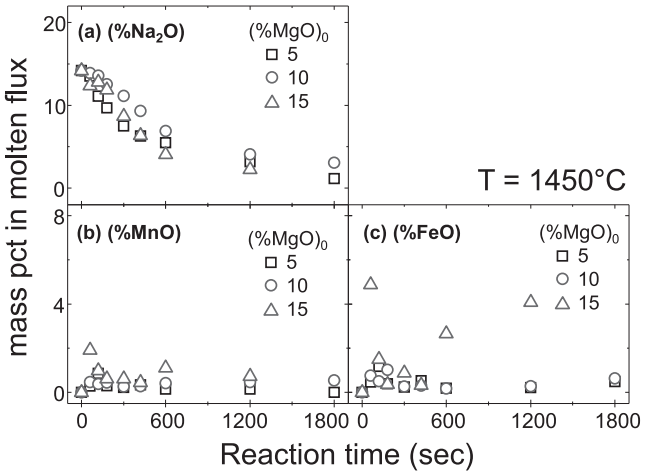


**Fig. 5.** Effect of (pct $MgO)_0$ on composition evolution of weak oxides in molten flux reacted with molten steel at 1 450°C: (a) (pct $Na_2O$), (b) (pct MnO), and (c) (pct FeO).

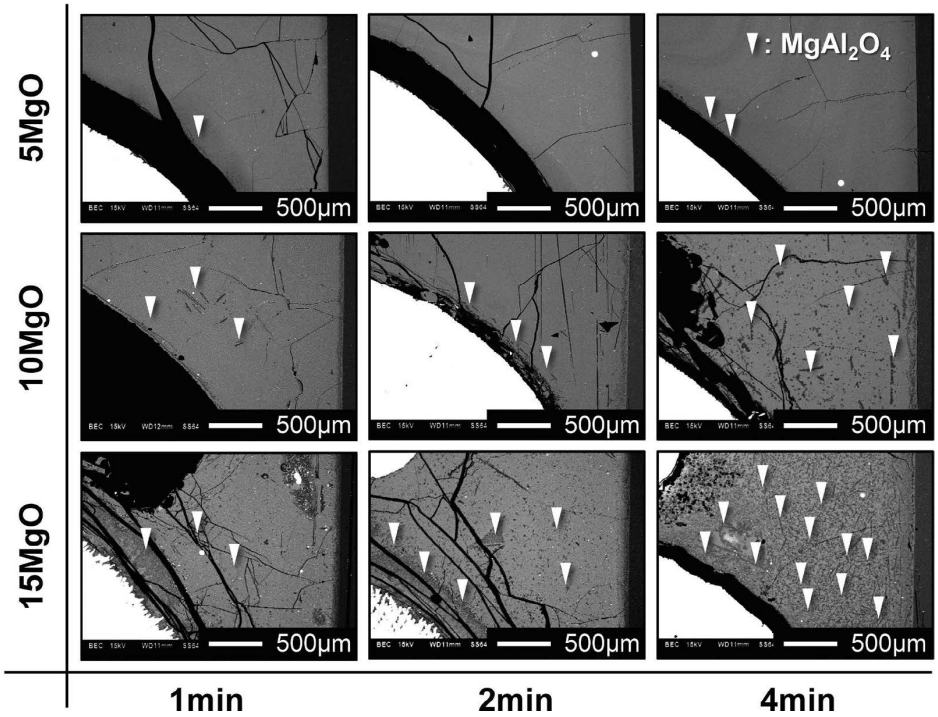


**Fig. 6.** Morphologies of the molten flux at different (pct $MgO)_0$ and reaction times showing $MgAl_2O_4$ formation.

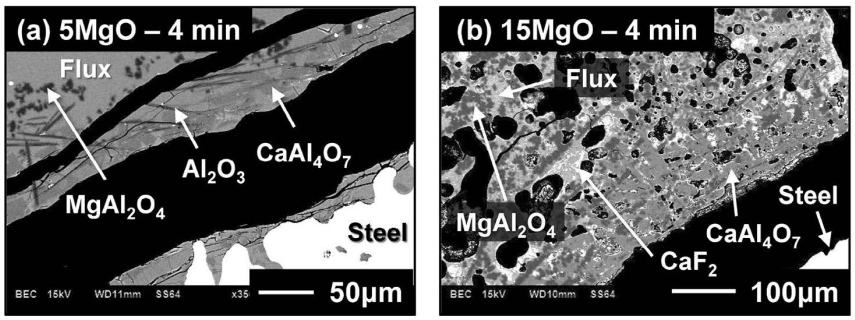


**Fig. 7.** Morphologies of the molten fluxes near steel-flux interface at 4 minutes of reaction time when (pct $MgO)_0$ was (a) 5 and (b) 15. $CaAl_4O_7$, $Al_2O_3$, and $CaF_2$ are observed.

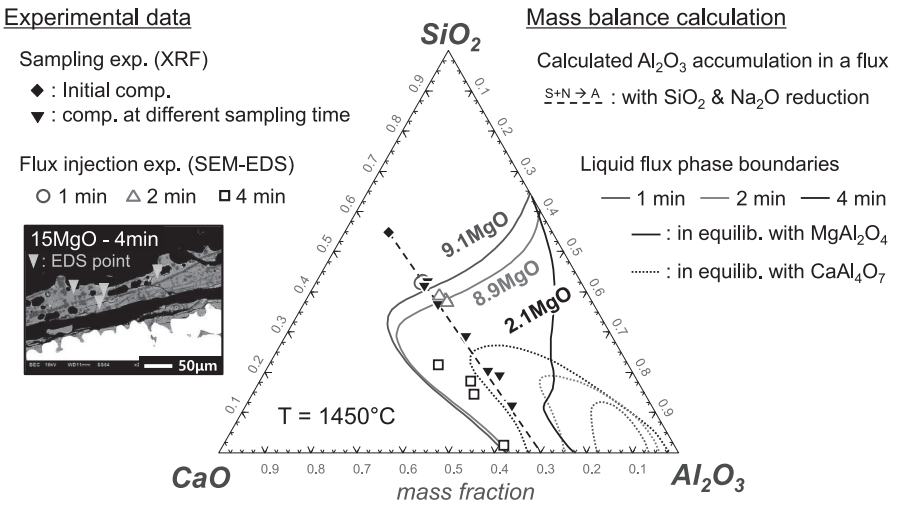


**Fig. 8.** Composition changes of molten flux measured by sampling experiment and flux injection experiment when (pct $MgO)_0$ was 15. Calculated CaO–$SiO_2$–$Al_2O_3$–MgO–$Na_2O$–F phase diagram by FactSage[16,17] is also shown for comparison.

of MgO content, while $Al_2O_3$ was continuously supplied with reduction of $SiO_2$ or $Na_2O$. This resulted in alumina or other aluminate formation in the flux. Those reaction products were formed as particles or as layers. Whatever was the shape of the reaction products, they should have affected mass transport in the flux, either by changing viscosity of remained flux, or by increasing apparent viscosity of the local flux-solid mixture. Therefore, it is important to understand formation mechanism of solid reaction products in the molten flux in order to explain how the mass transport in the flux could be changed with the rapid $Al_2O_3$ accumulation in the molten flux.

## 4. Discussions

### 4.1. Formation of $MgAl_2O_4$ Spinel Particles and Mass Transport in the Molten Flux

In order to examine whether the formation of $MgAl_2O_4$ has some effect on the mass transport phenomena in the flux, present experimental results of both sampling experiments and flux injection experiments were analyzed along with phase diagram of the flux system. The phase diagram was obtained by FactSage thermodynamic software.[16,17] FTOxid database was used. Phase diagrams of CaO–$SiO_2$–$Al_2O_3$–MgO–F systems were calculated, and are projected onto CaO–$SiO_2$–$Al_2O_3$ pseudo-ternary phase diagram. This was intended in order to focus on concentration changes of $Al_2O_3$ and $SiO_2$ in the flux. For the phase diagram calculations, other components such as MgO, $Na_2O$, and F (assuming in a form of $CaF_2$) were fixed to the concentrations obtained by SEM-EDS analysis at each reaction time. The stable aluminates observed in the samples are considered in the thermodynamic calculations. The calculated phase diagram for a flux of (pct $MgO)_0$ = 15 is shown in **Fig. 8**. During the reaction between the steel and the flux, $Al_2O_3$ accumulates in the flux, which then consumes MgO in the flux to form $MgAl_2O_4$. Therefore, MgO content in the flux gradually decreases marked by different colors (Please see the online version). Full lines represent composition of liquid flux in equilibrium with $MgAl_2O_4$, and dotted lines represent that with $CaAl_4O_7$.

Experimental data of (pct $MgO)_0$ = 15 were selected for comparison with the calculated phase diagram as shown in Fig. 8. Solid symbols are the experimental data obtained from the sampling experiment. This represents overall composition changes of the mixture of molten flux and aluminates. Open symbols are the other experimental data obtained from the flux injection experiment. This represents composition changes of molten flux after formation of aluminates. It is clearly seen that compositions of the molten flux nearby the steel-flux interface (open symbols) shows good agreement with the calculated phase boundary of molten flux in equilibrium with different aluminates. From SEM-EDS analysis, it was determined that MgO content in the molten flux near the steel-flux interface rapidly decreased due to $MgAl_2O_4$ formation. This local depletion

of MgO concentration in the flux results in shift of the liquid composition in equilibrium with $MgAl_2O_4$ phase as shown in the calculated phase diagram. Consequently, the molten flux can have high $Al_2O_3$ concentration by the formation of $MgAl_2O_4$ particles, and mass transport of $Al_2O_3$ from the interface to the bulk flux can occur successfully without forming subsequent $MgAl_2O_4$ due to decreased local MgO content. As MgO concentration in the flux decreased, however, calcium aluminate becomes stable, forming the calcium aluminate. This is consistent with the experimental observation. Composition change of molten flux from sampling experiments also shows the similar trend to the flux composition changes from flux injection experiments.

In addition to this, flux composition near the interface was further analyzed by WDS line analysis. The results are shown in **Fig. 9** for the sample of (pct MgO)$_0$ = 15. At the initial stage of steel-flux reaction, $Al_2O_3$ concentration increased with decrease of $SiO_2$ nearby the steel-flux interface, and narrow concentration gradient was observed. As the reaction proceeded, the concentration gradient becomes more remarkable, in particular for the $Al_2O_3$ and $SiO_2$. Many sharp intensity peaks corresponding mainly to $MgAl_2O_4$ particles were observed. And overall intensity of $SiO_2$ and MgO decreased while that of $Al_2O_3$ increased. From these observations, it is now evident that the reaction between the steel and the flux resulted in accumulation of $Al_2O_3$ near the interface, forming $MgAl_2O_4$ as well as developing concentration gradient in the flux.

### 4.2. Reaction Mechanism Investigation

In the previous investigation of the present authors,[2] it was concluded that rate controlling step of the Reaction (1) was mass transport of Al in the molten steel, at relatively low Al concentration ([pct Al]$_0$ ≤1.8) in the temperature range of 1 440°C to 1 550°C). It was experimentally confirmed that the flux did not show noticeable concentration gradient near the interface. On the other hand, when the Al concentration was high ([pct Al]$_0$ = 4.8), the reaction was not controlled by the mass transport of Al in the steel. In the present study for high Al content in steel and high MgO content in flux, it was shown that there was significant concentration gradient developed in the flux (Fig. 9), and many reaction product particles existed (Figs. 6 and 7). This observation mean the reaction rate would not be solely controlled by the mass transport of Al in the steel. Assuming rapid chemical reaction at the interface at high temperature, there is a possibility for mass transport in the flux phase to contribute to the rate controlling step.

**Figure 10** shows a simple kinetic analysis assuming the rate controlling step would still be the mass transport of Al in the liquid steel:

$$\frac{d[\text{pct Al}]}{dt} = -\frac{A\rho_{\text{steel}}}{W_{\text{steel}}} k_{\text{Al}}^{m}([\text{pct Al}] - [\text{pct Al}]^{i}) \quad \text{..... (5)}$$

By integrating the above equation, it is obtained:

$$\ln\frac{[\text{pct Al}] - [\text{pct Al}]_{\text{eq}}}{[\text{pct Al}]_0 - [\text{pct Al}]_{\text{eq}}} = -\frac{A\rho_{\text{steel}}}{W_{\text{steel}}} k_{\text{Al}}^{m}\alpha_{\text{Al}} t \quad \text{..... (6)}$$

where

$$\alpha_{\text{Al}} \equiv \frac{W_{\text{steel}}(M_{\text{Al}_2\text{O}_3}/2)[\text{pct Al}]_0 + W_{\text{flux}} M_{\text{Al}}(\text{pct Al}_2\text{O}_3)_0}{W_{\text{steel}}(M_{\text{Al}_2\text{O}_3}/2)([\text{pct Al}]_0 - [\text{pct Al}]_{\text{eq}}) + W_{\text{flux}} M_{\text{Al}}(\text{pct Al}_2\text{O}_3)_0} \quad \text{..... (7)}$$

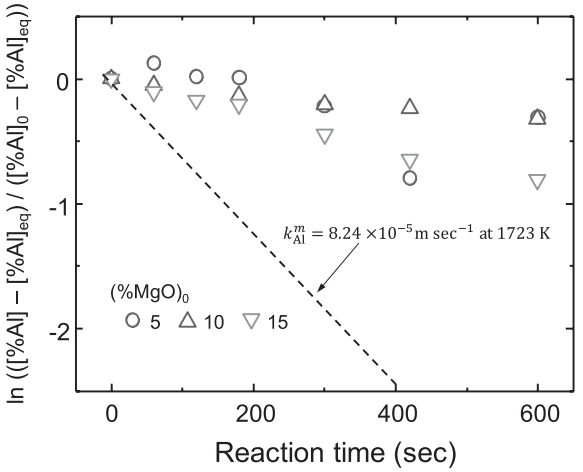


**Fig. 10.** Integrated rate plot of ln (([pct Al]−[pct Al]$_{eq}$)/([pct Al]$_0$−[pct Al]$_{eq}$)) with respect to reaction time under various (MgO)$_0$. Dashed line is calculated by using $k_{\text{Al}}^{m}$ derived in the previous study.[2]

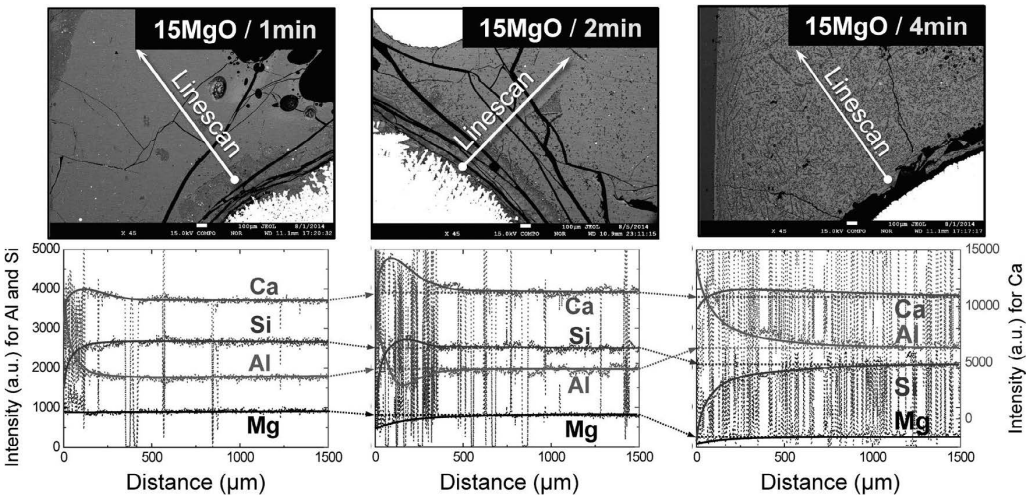


**Fig. 9.** Line scan analysis on the flux sample with 15 of (pct MgO)$_0$ showing considerable concentration gradient in the flux.

and $^{i}$, $_{0}$, and $_{eq}$ represent interface, initial, and equilibrium, respectively. $A$, $\rho_{steel}$, $W_{steel}$, $W_{flux}$, $k^{m}_{Al}$, $M_{Al}$, $M_{Al_2O_3}$ and $t$ are interfacial area, density of the steel, mass of the steel, mass of the flux, mass transport coefficient of Al in the steel, molecular weight of Al, molecular weight of $Al_2O_3$, and reaction time, respectively. Derivation steps for the Eqs. (6) and (7) are given in Appendix A.

Experimental data shown in Fig. 4(a) were replotted in the Fig. 10 by symbols. Dashed line in the figure was calculated using the Eq. (6). $A$ was estimated to be a cross-sectional area of the interior of the crucible. To the best knowledge of the present authors, density of the liquid Fe–C–Mn–Al alloys is not available in open literature. Therefore, as a first approximation, density was calculated by the equation proposed by Hoai and Lee[11] who measured volume of liquid Fe–C–Mn alloys at various temperatures. Contrary to the previous analysis,[2] the [pct Al]$_{eq}$ is not negligible in the present study due to higher Al content, therefore, it was taken into account in the present analysis. Data used for the calculation is given in **Table 3**. From the data shown in Fig. 4(a), $\alpha_{Al}$ was approximated to be 2–3. As can be seen in the figure, decrease of [pct Al] could not be explained by the assumed rate controlling step (mass transport of Al in the liquid steel). Experimental data clearly show that the rate was retarded, probably by additional resistance in the flux phase.

As discussed previously, the mass transport in the molten flux could contribute to the rate controlling step, because slow mass transport in the molten flux might resulted in concentration gradient in the flux. In order to examine the possibility of flux phase mass transfer control, the experimental data were analyzed by assuming flux phase mass transport control. If mass transport of $Al_2O_3$ in the flux might have controlled the reaction rate, then the $Al_2O_3$ accumulation rate may be formulated as:

$$\frac{d(\text{pct Al}_2\text{O}_3)}{dt} = \frac{A\rho_{flux}}{W_{flux}} k^{s}_{Al_2O_3}[(\text{pct Al}_2\text{O}_3)^{i} - (\text{pct Al}_2\text{O}_3)] \quad \text{..... (8)}$$

**Table 3.** Data used for calculation of mass transport coefficient in the present study.

| Symbol | Unit | Value | Note |
|---|---|---|---|
| $A$ | $m^2$ | $2.1 \times 10^{-3}$ | Cross-sectional area of crucible |
| $\rho_{steel}$ | kg $m^{-3}$ | $6.6 \times 10^{3}$ | Reference 11) |
| $\rho_{flux}$ | kg $m^{-3}$ | $2.6 \times 10^{3}$ | Reference 2) |
| $W_{steel}$ | kg | 0.4 | – |
| $W_{flux}$ | kg | 0.04 | – |
| [pct Al]$_0$ | – | 5 | – |
| [pct Al]$_{eq}$ | – | 2.8–3.5 | for different (pct MgO)$_0$ |
| (pct $Al_2O_3$)$_0$ | – | 6 | – |
| (pct $Al_2O_3$)$_{eq}$ | – | 40–45 | for different (pct MgO)$_0$ |
| [pct Si]$_0$ | – | $2 \times 10^{-2}$ | – |
| [pct Si]$_{eq}$ | – | 0.8 | for different (pct MgO)$_0$ |
| (pct $SiO_2$)$_0$ | – | 34.51 | – |
| (pct $SiO_2$)$_{eq}$ | – | 17 | for different (pct MgO)$_0$ |

By integrating the above equation, it is obtained:

$$\ln\frac{(\text{pct Al}_2\text{O}_3) - (\text{pct Al}_2\text{O}_3)_{eq}}{(\text{pct Al}_2\text{O}_3)_0 - (\text{pct Al}_2\text{O}_3)_{eq}} = -\frac{A\rho_{flux}}{W_{flux}}\alpha_{Al_2O_3} k^{s}_{Al_2O_3} t \quad \text{... (9)}$$

where

$$\alpha_{Al_2O_3} \equiv \frac{W_{steel}(M_{Al_2O_3}/2)[\text{pct Al}]_0 + W_{flux}M_{Al}(\text{pct Al}_2\text{O}_3)_0}{W_{steel}(M_{Al_2O_3}/2)[\text{pct Al}]_0 + W_{flux}M_{Al}((\text{pct Al}_2\text{O}_3)_0 - (\text{pct Al}_2\text{O}_3)_{eq})} \quad \text{..... (10)}$$

and $\rho_{flux}$, $k^{s}_{Al_2O_3}$ are density of the flux and mass transport coefficient of $Al_2O_3$ in the flux, respectively. Similarly, if mass transport of $SiO_2$ in the flux might have controlled the reaction rate, then the $SiO_2$ reduction rate may be formulated as:

$$\frac{d(\text{pct SiO}_2)}{dt} = -\frac{A\rho_{flux}}{W_{flux}} k^{s}_{SiO_2}[(\text{pct SiO}_2) - (\text{pct SiO}_2)^{i}] \quad \text{... (11)}$$

$$\ln\frac{(\text{pct SiO}_2) - (\text{pct SiO}_2)_{eq}}{(\text{pct SiO}_2)_0 - (\text{pct SiO}_2)_{eq}} = -\frac{A\rho_{flux}}{W_{flux}}\alpha_{SiO_2} k^{s}_{SiO_2} t \quad \text{... (12)}$$

where

$$\alpha_{SiO_2} \equiv \frac{W_{steel}M_{SiO_2}[\text{pct Si}]_0 + W_{flux}M_{Si}(\text{pct SiO}_2)_0}{W_{steel}M_{SiO_2}[\text{pct Si}]_0 + W_{flux}M_{Si}((\text{pct SiO}_2)_0 - (\text{pct SiO}_2)_{eq})} \quad \text{..... (13)}$$

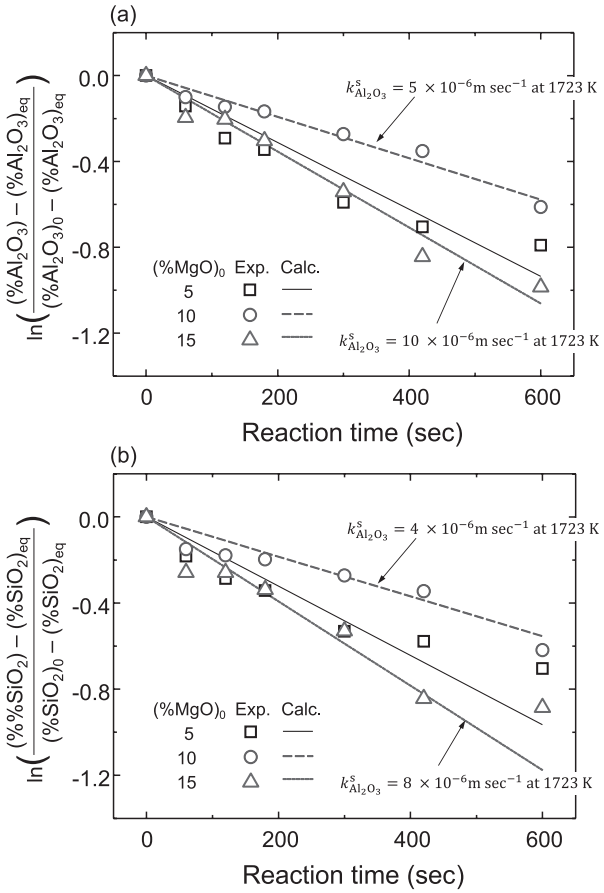


**Fig. 11.** Integrated rate plot for (a) mass transport of $Al_2O_3$ and (b) mass transport of $SiO_2$ in molten flux with high (pct MgO)$_0$ concentration. The apparent rate constant of $M_xO_y$ ($k^{s}_{M_xO_y}$) calculated from the slope are also shown in the figure.

Derivation steps for the Eqs. (9) and (12) are given in Appendix A.

The mass transfer coefficient of $Al_2O_3$ and $SiO_2$ obtained from the experimental data under 5 to 15 mass pct of $(\%MgO)_0$ in the flux are shown in **Fig. 11**. $k^s_{Al_2O_3}$ in the high MgO flux was estimated to be in the range of $5 \times 10^{-6}$ to $10 \times 10^{-6}$ m sec$^{-1}$, while $k^s_{SiO_2}$ shows similar values in the range of $4 \times 10^{-6}$ to $8 \times 10^{-6}$ m sec$^{-1}$. Data used for the calculation is given in Table 3. The $k^s_{Al_2O_3}$ and $k^s_{SiO_2}$ values estimated in the present study look to be in the similar range of those reported in literature.[12–15] Nevertheless, it is not thought to be very accurate values, because none of experimental data in Fig. 11 could be explained by a single rate controlling step. Moreover, the flux was not a homogeneous phase. Therefore, the reaction kinetic analyses in this section should not be considered as a quantitative result. Slopes varied as (pct MgO) varied. This might have been affected by formation of reaction products such as $MgAl_2O_4$ as was discussed in Sec. 4.1.

## 5. Conclusions

In order to investigate the reaction mechanism between high Mn–high Al steel and CaO–$SiO_2$-type flux at high Al concentration ($[\text{pct Al}]_0 = 5.2$) and high MgO concentration ($(\text{pct MgO})_0 = 5$ to 15), a number of steel–flux experiments were carried out with emphasis on the rate controlling step change.

In addition to reduction of $SiO_2$ by Al, considerable $Na_2O$ reduction by Al was confirmed. This should be considered to deteriorate of mold flux functions by increasing viscosity and affecting crystallization.

Microstructure observation on the steel-flux interface revealed that $MgAl_2O_4$ particles start to form near the steel-flux interface at the early stage of the reaction and appear in the bulk flux later. At the later stage of the reaction, other aluminates such as $CaAl_4O_7$ and $Al_2O_3$ were also observed due to local depletion of MgO in the flux. Regardless of the amount of $MgAl_2O_4$ particle formation in the molten flux, fast $Al_2O_3$ accumulation was determined from composition evolution in the molten flux under different $(\text{pct MgO})_0$ conditions.

$MgAl_2O_4$ formation mechanism and its effect on mass transport in the molten flux were discussed with consideration of compositions of the molten flux single phase near the $MgAl_2O_4$ particles, composition changes of the flux-aluminate mixture, and calculated phase diagrams. Development of concentration gradients observed from line scan analysis also suggested that flux composition changes are in close relationship with $MgAl_2O_4$ formation.

**Acknowledgement**

This research was financially supported by POSCO.

## REFERENCES

1) M.-S. Kim, S.-W. Lee, J.-W. Cho, M.-S. Park, H.-G. Lee and Y.-B. Kang: *Metall. Mater. Trans. B*, **44B** (2013), 299.
2) Y.-B. Kang, M.-S. Kim, S.-W. Lee, J.-W. Cho, M.-S. Park and H.-G. Lee: *Metall. Mater. Trans. B*, **44B** (2013), 309.
3) D.-J. Kim and J.-H. Park: *Metall. Mater. Trans. B*, **43B** (2012), 875.
4) S.-H. Kim, H. Kim and N. J. Kim: *Nature*, **518** (2015), 77.
5) H. Sun and K. Mori: *ISIJ Int.*, **36** (1996), S34.
6) M. A. Rhamdhani, K. S. Coley and G. A. Brooks: *Metall. Mater. Trans. B*, **36B** (2005), 219.
7) H. Ooi, T. Nozaki and H. Yoshii: *Trans. Iron Steel Inst. Jpn.*, **14** (1974), 9.
8) J. Park, S. Sridhar and R. J. Fruehan: *Metall. Mater. Trans. B*, **45B** (2014), 1380.
9) K. Blazek, H. Yin, G. Skoczylas, M. McClymonds and M. Frazee: 7th European Continuous Casting Conf. (ECCC), Steel Institute VDEh, Düsseldorf, Germany, (2011), 1.
10) J.-W. Cho, K. Blazek, M. Frazee, H. Yin, J.-H. Park and S.-W. Moon: *ISIJ Int.*, **53** (2013), 62.
11) L. Thu Hoai and J. Lee: *Metall. Mater. Trans. B*, **42B** (2011), 925.
12) J.-Y. Choi, H.-G. Lee and J.-S. Kim: *ISIJ Int.*, **42** (2002), 852.
13) M. Umakoshi, K. Mori and Y. Kawai: *Tetsu-to-Hagané*, **67** (1981), 1726.
14) J.-K. Jung and J.-J. Pak: *J. Kor. Inst. Met. Mater.*, **38** (2000), 585.
15) B. J. Monaghan, R. J. Pomfret and K. S. Coley: *Metall. Mater. Trans. B*, **29B** (1998), 111.
16) C. W. Bale, É. Belisle, P. Chartrand, S. Degterov, G. Eriksson, K. Hack, I.-H. Jung, Y.-B. Kang, J. Melançon, A. D. Pelton, C. Robelin and S. Petersen: *Calphad*, **33** (2009), 295.
17) C. W. Bale, É. Belisle, P. Chartrand, S. Degterov, G. Eriksson, A. Gheribi, K. Hack, I.-H. Jung, Y.-B. Kang, J. Melançon, A. D. Pelton, S. Petersen, C. Robelin, J. Sangster, P. Spencer and M.-A. Van Ende: *Calphad*, **54** (2016), 35.

## Appendix A

### Rate Equations when Mass Transport of a Species Controls the Reaction Rate

This section provides derivation steps for the rate equations (Eqs. (6), (9), and (12)) used in Sec. 4.2. It is assumed that there are only two phases (steel and flux), no third phase is considered, and chemical equilibrium at the interface is assumed. Reaction rate is controlled either by mass transport of a species X in a boundary layer of the steel, or by mass transport of a species $XO_x$ in the other boundary layer of the flux.

### A.1. When Mass Transport of X in Liquid Steel Controls the Reaction Rate

In this case, there is a concentration gradient in the steel phase ($[\text{pct X}] \neq [\text{pct X}]^i$), but no concentration gradient is assumed in the flux phase ($(\text{pct XO}_x) = (\text{pct XO}_x)^i$). The equilibrium is assumed:

$$L = \frac{(\text{pct XO}_x)^i}{[\text{pct X}]^i} = \frac{(\text{pct XO}_x)}{[\text{pct X}]^i} \quad \text{..... (A1)}$$

where $L$ is the equilibrium partition coefficient. The above relationship should be hold when the two phases approach at the equilibrium. Therefore,

$$L = \frac{(\text{pct XO}_x)}{[\text{pct X}]^i} = \frac{(\text{pct XO}_x)_{eq}}{[\text{pct X}]_{eq}} \quad \text{..... (A2)}$$

Reaction rate is formulated as:

$$\frac{d[\text{pct X}]}{dt} = -\frac{A}{V_{steel}} k^m_X ([\text{pct X}] - [\text{pct X}]^i) \quad \text{..... (A3)}$$

By mass conservation in the two phase system, it is hold:

$$[(\text{pct X})_0 - [\text{pct X}]) \frac{W_{steel}}{M_X} = ((\text{pct XO}_x) - (\text{pct XO}_x)_0) \frac{W_{flux}}{M_{XO_x}} \quad \text{..... (A4)}$$

For the above relationship, $W_{steel}$ and $W_{flux}$ are assumed not to vary during the reaction. By using the mass conservation,

$$(\text{pct XO}_x) = (\text{pct XO}_x)_0 + \frac{W_{\text{steel}} M_{\text{XO}_x}}{W_{\text{flux}} M_{\text{X}}}([\text{pct X}]_0 - [\text{pct X}]) \quad \text{..... (A5)}$$

$$(\text{pct XO}_x)_{\text{eq}} = (\text{pct XO}_x)_0 + \frac{W_{\text{steel}} M_{\text{XO}_x}}{W_{\text{flux}} M_{\text{X}}}([\text{pct X}]_0 - [\text{pct X}]_{\text{eq}}) \quad \text{..... (A6)}$$

From the Eq. (A2),

$$[\text{pct X}]^i = \frac{[\text{pct X}]_{\text{eq}}}{(\text{pct XO}_x)_{\text{eq}}}(\text{pct XO}_x) \quad \text{..... (A7)}$$

Substituting the Eqs. (A5) and (A6) into the Eq. (A7), and subsequent substitution into Eq. (A3) results in:

$$\frac{d[\text{pct X}]}{dt} = -\frac{A}{V_{\text{steel}}} k_{\text{X}}^m \alpha_{\text{X}} ([\text{pct X}] - [\text{pct X}]_{\text{eq}}) \quad \text{.... (A8)}$$

where

$$\alpha_{\text{X}} \equiv \frac{M_{\text{XO}_x} W_{\text{steel}} [\text{pct X}]_0 + M_{\text{X}} W_{\text{flux}} (\text{pct XO}_x)_0}{M_{\text{XO}_x} W_{\text{steel}} ([\text{pct X}]_0 - [\text{pct X}]_{\text{eq}}) + M_{\text{X}} W_{\text{flux}} (\text{pct XO}_x)_0} \quad \text{..... (A9)}$$

Integration of the above equation yields:

$$\ln \frac{[\text{pct X}] - [\text{pct X}]_{\text{eq}}}{[\text{pct X}]_0 - [\text{pct X}]_{\text{eq}}} = -\frac{A}{V_{\text{steel}}} k_{\text{X}}^m \alpha_{\text{X}} t \quad \text{..... (A10)}$$

### A.2. When Mass Transport of $XO_x$ in Liquid Flux Controls the Reaction Rate

In this case, [pct X] = [pct X]$^i$ while (pct $XO_x$) ≠ (pct $XO_x$)$^i$. The equilibrium is assumed:

$$L = \frac{(\text{pct XO}_x)^i}{[\text{pct X}]^i} = \frac{(\text{pct XO}_x)^i}{[\text{pct X}]} = \frac{(\text{pct XO}_x)_{\text{eq}}}{[\text{pct X}]_{\text{eq}}} \quad \text{...(A11)}$$

Reaction rate is formulated as:

$$\frac{d(\text{pct XO}_x)}{dt} = -\frac{A}{V_{\text{flux}}} k_{\text{XO}_x}^s ((\text{pct XO}_x) - (\text{pct XO}_x)^i) \quad \text{... (A12)}$$

By using the mass conservation,

$$[\text{pct X}] = [\text{pct X}]_0 + \frac{W_{\text{flux}} M_{\text{X}}}{W_{\text{steel}} M_{\text{XO}_x}}((\text{pct XO}_x)_0 - (\text{pct XO}_x)) \quad \text{..... (A13)}$$

$$[\text{pct X}]_{\text{eq}} = [\text{pct X}]_0 + \frac{W_{\text{flux}} M_{\text{X}}}{W_{\text{steel}} M_{\text{XO}_x}}((\text{pct XO}_x)_0 - (\text{pct XO}_x)_{\text{eq}}) \quad \text{... (A14)}$$

From the Eq. (A11),

$$(\text{pct XO}_x)^i = \frac{(\text{pct XO}_x)_{\text{eq}}}{[\text{pct X}]_{\text{eq}}}[\text{pct X}] \quad \text{..... (A15)}$$

Substituting the Eqs. (A13) and (A14) into the Eq. (A15), and subsequent substitution into Eq. (A12) results in:

$$\frac{d(\text{pct XO}_x)}{dt} = -\frac{A}{V_{\text{flux}}} k_{\text{XO}_x}^s \alpha_{\text{XO}_x} ((\text{pct XO}_x) - (\text{pct XO}_x)_{\text{eq}}) \quad \text{..... (A16)}$$

where

$$\alpha_{\text{XO}_x} \equiv \frac{M_{\text{XO}_x} W_{\text{steel}} [\text{pct X}]_0 + M_{\text{X}} W_{\text{flux}} (\text{pct XO}_x)_0}{M_{\text{XO}_x} W_{\text{steel}} [\text{pct X}]_0 + M_{\text{X}} W_{\text{flux}} ((\text{pct XO}_x)_0 - (\text{pct XO}_x)_{\text{eq}})} \quad \text{..... (A17)}$$

Integration of the above equation yields:

$$\ln \frac{(\text{pct XO}_x) - (\text{pct XO}_x)_{\text{eq}}}{(\text{pct XO}_x)_0 - (\text{pct XO}_x)_{\text{eq}}} = -\frac{A}{V_{\text{flux}}} k_{\text{XO}_x}^s \alpha_{\text{XO}_x} t \quad \text{... (A18)}$$